Carbonate platform production during the Cretaceous.

Alexandre Pohl, Yannick Donnadieu, Yves Godderis, Cyprien Lanteaume, Alex Hairabian, Camille Frau, Julien Michel, Marie Laugie, John J.G. Reijmer, Christopher R. Scotese, et al.

Carbonate platform production during the Cretaceous

Alexandre POHL[1,2,3], Yannick DONNADIEU[1], Yves GODDERIS[4], Cyprien LANTEAUME[1,5,6], Alex HAIRABIAN[7], Camille FRAU[1], Julien MICHEL[1, 5], Marie LAUGIE[1], John J. G. REIJMER[7], Christopher R. SCOTESE[8], Jean BORGOMANO[1].

[1]Aix Marseille Univ, CNRS, IRD, Coll France, INRA, CEREGE. Aix-en-Provence, France

[2]Department of Earth Sciences, University of California, Riverside, CA, USA

[3]Biogéosciences, UMR 6282, UBFC/CNRS, Université Bourgogne Franche-Comté, 6 boulevard Gabriel, F-21000 Dijon, France

[4]UMR5563 Géosciences Environnement Toulouse, Observatoire Midi-Pyrénées, CNRS, Toulouse, France

[5]MODIS Pau, 4 Rue Jules Ferry, Pau, France

[6]Total CSTJF, Avenue Larribeau, 64000 Pau, France

[7]College of Petroleum Engineering & Geosciences, King Fahd University of Petroleum & Minerals, Dhahran 31261, Saudi Arabia

[8]Department of Earth & Planetary Sciences, Northwestern University, Evanston, IL, 60201, USA

ABSTRACT

Platform carbonates are among the most voluminous of Cretaceous deposits. The production of carbonate platforms fluctuated through time. Yet, the reasons for these fluctuations are not well understood and the underlying mechanisms remain largely unconstrained. Here we document the long-term trend in Cretaceous carbonate platform preservation based on a new data compilation and use a climate-carbon cycle model to explore the drivers of carbonate platform production during the Cretaceous. We show that neritic carbonate preservation rates followed a

unimodal pattern during the Cretaceous reaching maximum values during the mid Cretaceous (Albian, 110 Ma). Coupled climate-carbon cycle modeling reveals that this maximum in carbonate deposition results from a unique combination of high volcanic degassing rates and widespread shallow-marine environments that served as a substrate for neritic carbonate deposition. Our experiments demonstrate that the unimodal pattern in neritic carbonate accumulation agrees well with most of the volcanic degassing scenarios for the Cretaceous. Our results suggest that the first-order temporal evolution of neritic carbonate production during the Cretaceous reflects changes in continental configuration and volcanic degassing. Geodynamics, by modulating accommodation space, and turnovers in the dominant biota probably played a role as well, but it is not necessary to account for the latter processes to explain the first-order trend in Cretaceous neritic carbonate accumulation in our simulations.

INTRODUCTION

In the recent years, our knowledge of the geological evolution of the surficial carbon cycle has greatly improved. Among the main advances is the reconstruction of the Phanerozoic atmospheric CO_2 (Berner, 2006; Foster et al., 2017). The fluctuations of the carbon sink due to continental weathering as well as the change in solid Earth degassing have been at least partly constrained, using models (Goddéris et al., 2014; Brune et al., 2017) or proxies (such as isotopes) (Veizer et al., 1999; Cao et al., 2017). One major component of the carbon cycle, however, the sedimentary carbonate sink, has been poorly investigated at the global scale. Many data have been published, regarding carbonate accumulation fluxes (Bosscher and Schlager, 1993; Kiessling et al., 2000), but data compilations and extrapolation at the global scale are scarce.

Carbonate sediments are the receptacle of the atmospheric CO_2 that has been removed from the atmosphere by weathering, which can be subsequently recycled along subduction zones

47 (Mason et al., 2017; Pall et al., 2018). Carbonate sediment deposition thus reflects many coupled
48 processes. Identifying those processes through geological times is an unparalleled way to check
49 whether we have understood the overall functioning of the carbon cycle or not.

50 Here we investigate the production by carbonate platforms during the Cretaceous, one of
51 the most prolific periods of carbonate platform development (Kiessling et al., 2003). We
52 reconstruct temporal variations in platform carbonate deposition based on a new data
53 compilation and subsequently explore the drivers of the temporal trends in Cretaceous carbonate
54 production using a coupled climate-carbon cycle model.

55 **METHODS**

56 **Database of shallow-water carbonate preservation rates**

57 We compiled, from published studies, an extensive database of Cretaceous shallow-water
58 marine carbonate preservation rates (see the GSA Data Repository for the full database). The
59 latter were calculated by dividing the estimated sediment thickness by the stratigraphic interval
60 duration. Calculated preservation rates necessarily underestimate actual carbonate production
61 rates. Indeed, neritic carbonate accumulation is limited by depositional accommodation space. In
62 addition, deposits may subsequently undergo dissolution, erosion and compaction, and produced
63 sediments may be exported toward the basin. As a result of all those mechanisms acting to
64 reduce the thickness of the carbonates preserved on the shelves, preservation rates calculated
65 based on the geological record are typically one to several orders of magnitude lower than
66 production rates measured on present-day carbonate-secreting ecosytems such as coral reefs
67 (Bosscher, 1992; Strasser and Samankassou, 2003; Schlager, 2010). Therefore compiled
68 preservation rates are considered significant underestimations of the actual accumulation rates.
69 Considering the multiple mechanisms acting to reduce the thickness of the shallow-water

carbonates preserved on the shelves, maximum preservation rates are further considered to be the most representative of the original carbonate accumulation flux in ancient times.

The GEOCLIM climate-carbon cycle model

We used the GEOCLIM climate-carbon cycle model (see the Data Repository) to simulate carbonate accumulation fluxes during the Cretaceous. The GEOCLIM model (Donnadieu et al., 2006a) asynchronously couples a carbon cycle box model with a general circulation model. It represents a significant improvement over the zero-dimensional GEOCARB-like models (Berner, 2006), since continental weathering rates are resolved spatially, which takes into account the continental configuration and sea level (Goddéris et al., 2014). The carbon cycle box model is the COMBINE model upgraded following Donnadieu et al. (2006a). It includes a robust representation of the marine sub-cycles of inorganic and organic carbon, oxygen, alkalinity and phosphorus. It explicitly represents the spatial distribution of silicate, basalt and carbonate weathering as a function of climate. The oceans are modeled by 9 "boxes". The accumulation of neritic carbonates takes place exclusively in the box representing the low-to-mid latitude epicontinental photic zone, following Eqn. 1:

$$\boldsymbol{F = k_{cr} \times A_{platform} \times (\Omega_{ara} - 1)^{1.7}} \quad (1)$$

where F is the neritic carbonate depositional flux (mol yr^{-1}), $A_{platform}$ is the shelf area available to shallow-water carbonate deposition, derived from the paleogeographic reconstructions, $\boldsymbol{\Omega}_{ara}$ is the model aragonite solubility ratio and k_{cr} a calibration constant. This formulation of neritic carbonate accumulation rates has been successfully used in previous studies to investigate the consequences of the demise of carbonate platforms during the Middle–Late Jurassic Transition (ca. 160 Ma; Donnadieu et al., 2011) and the effects of the breakup of Pangea on neritic carbonate accumulation (Late Permian to Late Cretaceous; Donnadieu et al.,

2006a). The climatic component of GEOCLIM is the FOAM ocean-atmosphere model version 1.5 (Jacob, 1997), a mixed-resolution general circulation model that has been routinely used to study climate in deep time, including during the Cretaceous (Donnadieu et al., 2006b; Ladant and Donnadieu, 2016).

Simulations were conducted using the Cretaceous paleogeographical reconstructions of Scotese (2016) and Scotese and Wright (2018) with deep-ocean bathymetry after Müller et al. (2008). Changing solar luminosity values were modeled after the stellar physics of Gough (1981). Earth's orbit around the Sun was circular (null eccentricity) and the obliquity was set to 22°. This orbital configuration provides an equal, annual insolation for both hemispheres with minimal seasonal contrast.

RESULTS

Temporal variations in Cretaceous shallow-water carbonate preservation rates

At first order, Fig. 1 shows a unimodal pattern in neritic carbonate preservation rates during the Cretaceous with background values < 70 m Myr^{-1} and an excursion to higher preservation rates up to 175–200 m Myr^{-1} during the mid Cretaceous between 125 Ma (Aptian) and 95 Ma (Cenomanian). This mid-Cretaceous maximum is a robust feature. It was already highlighted by the previous Phanerozoic compilation of Bosscher and Schlager (1993). It parallels the mid-Cretaceous local maximum in reefal carbonate production identified by Kiessling et al. (2000). It also corresponds with the development of massive successions of sediments in the Mediterranean Tethys (>100 m thick; Skelton and Gili, 2011) and with the maximum in carbonate accumulation identified in the North American, Russian and Siberian platforms (Whitten, 1976).

Coupled climate-carbon cycle simulations

116 The drivers of secular change in platform carbonate production have been the subject of
117 investigation for decades (Schlager, 1981; Bosscher and Schlager, 1993; Kiessling et al., 2000;
118 Donnadieu et al., 2006a). From a carbon cycle perspective, global carbonate deposition is tightly
119 linked to changes in continental silicate and carbonate weathering. However, several factors
120 impact the distribution of carbonate deposition between the open ocean and shallow-marine
121 platforms. Debate thus continues as to whether fluctuations in neritic carbonate accumulation
122 rates reflect changing environmental conditions such as global climate, evolving geodynamics
123 (e.g., continental configuration and subsidence) or intrinsic changes such as turnovers in
124 dominant biota, since different carbonate factories are known to be associated with different
125 carbonate production rates (e.g., Lanteaume et al., 2018). Previous attempts to identify these
126 complex relationships over the course of the Phanerozoic failed to reach any definitive
127 conclusions (Bosscher and Schlager, 1993; Kiessling et al., 2000).

128 ***Baseline simulations with present-day volcanism***

129 We used the GEOCLIM climate-carbon cycle model (Donnadieu et al., 2006a) to
130 investigate the driving mechanisms for the Cretaceous trend in neritic carbonate deposition with
131 a special focus on the maximum in carbonate accumulation centered at 110 Ma (see Fig. 1).
132 Simulations were run every 10 Myrs between 150 Ma (Late Jurassic) and 60 Ma (Paleocene).
133 For each time slice and associated continental configuration, the GEOCLIM model computed the
134 pCO_2 value by balancing volcanic degassing with silicate weathering. The GEOCLIM model
135 simulated the associated climatic state and ocean biogeochemistry. Though the neritic carbonate
136 deposition rate was focus of our investigation, the simulated pCO_2 was used to evaluate the fit of
137 our simulations to the latest pCO_2 reconstruction of Foster et al. (2017). The latter criterion was

chosen to compare our simulations to proxy data due to the critical role that pCO_2 plays on ocean pH and thus carbonate geochemistry.

In our baseline runs, the rate of volcanic degassing was set to the present-day value (6.8×10^{12} moles of carbon per year; Donnadieu et al., 2006a) (Fig. 2A); only the paleogeography and associated climate varied from one time slice to another. Simulated pCO_2 was lower than indicated by the proxy compilation for most of the Cretaceous (Fig. 2B). Yet, an interesting pattern emerged: the bimodal trend observed in the pCO_2 compilation between 120 Ma and 60 Ma (grey shading in Fig. 2B) was well reproduced in the baseline runs (black line in Fig. 2B). This suggests that the temporal variations in pCO_2 reconstructed by Foster et al. (2017) between 120 Ma and 60 Ma may be largely due to the paleogeographical evolution. The total neritic carbonate depositional flux simulated in the baseline runs varied very little between 150 Ma and 60 Ma, showing only a local optimum at 80 Ma (Fig. 2C).

Numerical simulations using Cretaceous volcanic degassing scenarios

In a second step, we used Cretaceous plate models and data compilations to derive volcanic CO_2 degassing scenarios, which could help reconcile the simulations with proxy-based pCO_2 reconstructions. Such modeling attempt faces limitations associated with the large uncertainties in the reconstruction of Cretaceous volcanic degassing. Indeed, numerous studies have been published trying to reconstruct one of the components of the degassing rate but there is no reconstruction of the total CO_2 degassing by the solid Earth at the geological timescale. The lack of an integrated curve leaves us with the necessity to rely on incomplete reconstructions. Such bias concerns both the modeling and data communities. For instance, McKenzie et al. (2016) argue for a dominant role of degassing on the climatic evolution, based on a correlation

between the Phanerozoic climate and their curve for the degassing of arc volcanism, although arc volcanism is only one component of the total degassing.

The rationale that we adopted thus consists in using available constraints to compute total volcanic degassing rates, expressed as ratios compared to the present-day value. We did not try to identify the individual contributions of the different components: subduction zones, rifts, mid-ocean ridges and arc volcanism. Instead, we followed the approach adopted by Berner in his various versions of the seminal GEOCARB(SULF) model (Berner and Kothavala, 2001; Berner, 2004, 2006), which consists in scaling volcanic degassing with proxies for geodynamic activity (e.g., subduction length). Although this approach will undoubtedly benefit from advances in geodynamic models in the near future, it has been shown to produce very good results in the GEOCARB model (Berner, 2006; Van Der Meer et al., 2014). In detail, we derived volcanic degassing rates (Fig. 2A) from the length of subduction zones calculated by Van Der Meer et al. (2014) (hereafter VDM14), from the area of subducted lithosphere reconstructed over the last 180 Myrs by Engebretson et al. (1992) (E92), from the slab flux estimated by East et al. (2020) (EA20) and from the continental arc activity compiled by Cao et al. (2017) (CAO17). We also used the C1' and C1'' scenarios of Brune et al. (2017), which consider variable contributions of rifts, mid-ocean ridges, subduction zones and continental arcs.

Our model does not account for the degassing from large igneous provinces (LIPs). It has been shown (Dessert et al., 2001) that LIP degassing increases the atmospheric partial pressure of CO_2 for durations that do not exceed a few million years after the end of the onset. LIPs also impact the carbonate system through short-term acidification of the ocean, just prior to the response of the weathering system (Paris et al., 2016). However, we here explore the response of the carbon cycle to processes acting at a longer timescale, in the order of ten million years.

We tested each of the volcanic degassing scenarios in the GEOCLIM model. The best fit to proxy data was obtained using the subduction-based degassing scenario E92 (Fig. 2B). The neritic carbonate production flux associated with this best-guess scenario displayed a maximum centered on 110 Ma (Fig. 2C) that agreed well with our compilation of Cretaceous preservation rates (see Fig. 1).

Analyzing the drivers of the Mid-Cretaceous maximum in carbonate accumulation

Despite the disparities in the volcanic degassing scenarios (Fig. 2A), most simulations showed that the highest rates of neritic carbonate production occurred during the mid Cretaceous (between ca. 120 and 80 Ma). The mid-Cretaceous unimodal pattern, bounded by an increase in neritic carbonate production in the Early Cretaceous (120-130 Ma) and a decrease in neritic carbonate production in the early Late Cretaceous (80 Ma), was a robust pattern that was shared by different degassing scenarios.

Comparison of the simulations that considered evolving volcanic degassing rates with the baseline runs (color vs. black lines in Fig. 2C) revealed that the lowest-to-mid Cretaceous increase in neritic carbonate production (130–120 Ma), at least partially, relied on an increase in volcanic degassing rates. In addition, a sensitivity test that used a constant area of the neritic environments available for carbonate deposition (dashed magenta line in Fig. 2C) demonstrated that the latter area played a key role in the increase in shallow-marine carbonate production. Indeed, the area of the continental shelves significantly rose between 130 Ma and 120 Ma in our reconstructions (Fig. 3). This increase resulted from the strong eustatic rise that took place at that time (Müller et al., 2008). In the E92 scenario, the increasing area of shallow-marine environments strengthened the pattern of carbonate accumulation already imposed by changing volcanism (Fig. 2C), by favoring the accumulation of carbonate in neritic environments at the

206 expense of the open ocean. In other degassing scenarios that did not have a well-defined
207 maximum at 120–110 Ma (i.e., C1', C1'', VDM14, CAO17, EA20), the increasing area of the
208 shallow-marine environments, alone, drove the increase in neritic carbonate production between
209 130 and 120 Ma (Figs. 2A,C). Regarding the decrease in carbonate production after 80 Ma, two
210 main mechanisms were in play; most scenarios showed a drop in volcanic degassing (Fig. 2A)
211 and a major eustatic fall (Müller et al., 2008) reduced the area of the shallow-marine
212 environments available to neritic carbonate deposition (Fig. 3).

213 **DISCUSSION**

214 Comparison of our simulated trend of shallow-water carbonate production with the
215 updated compilation of preservation rates allowed us to propose a mechanistic explanation to
216 temporal variations in the deposition of Cretaceous shallow-water carbonates. It would be even
217 more interesting and straightforward to compare our simulated fluxes with the volumes (instead
218 of vertical aggradation rates) of shallow-water carbonates produced during the Cretaceous.
219 Unfortunately, such comparison is hampered by the lack of robust quantification of these
220 volumes. For instance, Dutkiewicz et al. (2019) calculated platform carbonate accumulation
221 fluxes by multiplying the extent of the carbonate platforms mapped by Kiessling et al. (2003) by
222 globally-uniform preservation rates derived from the compilation of Bosscher and Schlager
223 (1993). Figure 1C reveals that the temporal trends of carbonate production simulated in
224 GEOCLIM and the preserved volumes reconstructed by Dutkiewicz et al. (2019) largely differ.
225 The estimates of Dutkiewicz et al. (2019) provide significantly lower values. The low values at
226 least partly reflect the action of dissolution, erosion, compaction and the export of the carbonates
227 toward the basin, which all tend to reduce the thickness of the carbonates deposited on the
228 shelves. Preserved volumes necessarily represent an underestimation of the volumes of carbonate

actually produced (see Methods). Regarding the temporal trend, the reconstruction of Dutkiewicz et al. (2019) does not provide any robust quantification of the variation in the production of platform carbonates. Indeed, the approach of Dutkiewicz et al. (2019) consists in multiplying the surface of the carbonate platforms documented in the geological database by a constant (i.e., a uniform rate of vertical aggradation). The authors derived two values for this constant rate from the compilation of Bosscher and Schlager (1993), which provided the lower (using 30 m Myr^{-1}) and upper (using 80 m Myr^{-1}) boundaries for their reconstructed trend (Fig. 1C). Our updated compilation of preservation rates (Fig. 1), however, reveals that preservation rates cover a very large range of values, from < 10 to 200 m Myr^{-1}. While it probably reflects the best estimate that can be produced at the global scale based on the current knowledge, the approach employed by Dutkiewicz et al. (2019) neglects the spatio-temporal variations in carbonate accumulation rates and thus exclusively reflects the evolution of the area of the carbonate platforms (compare Fig. 1C and Fig. 3). Skelton (2003) conducted similar calculations for the Aptian and Cenomanian. Only the platforms of the Tethyan region were considered in these calculations, while Dutkiewicz et al. (2019) considered the area of the platforms at the global scale. The fact that both studies led to virtually identical values (Fig. 1C), although they focused on significantly different spatial scales, highlights once again the difficulty to estimate the depositional flux by neritic carbonates in the deep time. We argue that, considering the current difficulty to estimate volumes of neritic carbonates produced in ancient times, our reconstructed neritic carbonate preservation rates (Fig. 1) constitute an instructive proxy for the efficiency of the shallow-water carbonate factory in ancient times. The reported temporal patterns are supported by both previous data compilations (Whitten, 1976; Bosscher and Schlager, 1993; Kiessling et al., 2000) and accumulation patterns observed in the field (Skelton and Gili, 2011).

CONCLUSION

The simulated maximum in mid-Cretaceous neritic carbonate production results from the combination of high volcanic degassing levels and the large shallow-marine realms. Although the precise evolution of carbonate accumulation rates varies from one volcanic degassing scenario to another, the unimodal pattern in neritic carbonate production simulated during the Cretaceous is robust and shows up in most of the scenarios. The model results align well with the temporal trend that emerges from the updated compilation of Cretaceous platform carbonate preservation rates. Our results therefore suggest that the first-order evolution of neritic carbonate deposition during the Cretaceous reflects changes in continental configuration and volcanic degassing. Other mechanisms modulating accommodation space and turnovers in the dominant biota probably played a role as well, but our simulations suggest that the latter processes do not explain the first-order trend in Cretaceous neritic carbonate accumulation.

ACKNOWLEDGMENTS

The authors thank Dietmar Müller, Peter Skelton and two anonymous reviewers for their thorough reviews that significantly strengthened the present manuscript, and Judith Totman Parrish and Gerald Dickens for editorial handling. A.P. and Y.D. thank the CEA/CCRT for providing access to the HPC resources of TGCC under the allocation 2014–012212 made by GENCI. The research leading to these results was supported by a Marie Sklodowska-Curie International Fellowship under Grand Agreement no. 838373. The authors thank B. Suchéras-Marx (CEREGE) for interesting discussions on the calcifying plankton during the Cretaceous, P. Maffre (GET) for his assistance in setting-up our Cretaceous configuration of the GEOCLIM model and S. Brune for providing degassing scenarios.

REFERENCES CITED

Berner, R.A., 2006, GEOCARBSULF: A combined model for Phanerozoic atmospheric O2 and CO2: Geochimica et Cosmochimica Acta, v. 70, p. 5653–5664, http://www.sciencedirect.com/science/article/pii/S0016703706002031.

Berner, R.A., 2004, The phanerozoic carbon cycle CO2 s and O2: New York, Oxford University Press.

Berner, R.A., and Kothavala, Z., 2001, GEOCARB III: a revised model of atmospheric CO2 over Phanerozoic time: American Journal of Science, v. 301, p. 182–204, http://ajsonline.org/content/301/2/182.short.

Bosscher, H., 1992, Growth potential of coral reefs and carbonate platforms: 157 p. p.

Bosscher, H., and Schlager, W., 1993, Accumulation rates of carbonate platforms: Journal of Geology, v. 101, p. 345–355, doi:10.1086/648228.

Brune, S., Williams, S.E., and Müller, R.D., 2017, Potential links between continental rifting, CO2 degassing and climate change through time: Nature Geoscience, v. 10, p. 941–946, doi:10.1038/s41561-017-0003-6.

Cao, W., Lee, C.-T.A., and Lackey, J.S., 2017, Episodic nature of continental arc activity since 750 Ma: A global compilation: Earth and Planetary Science Letters, v. 461, p. 85–95.

Dessert, C., Dupré, B., François, L.M., Schott, J., Gaillardet, J., Chakrapani, G., and Bajpai, S., 2001, Erosion of Deccan Traps determined by river geochemistry: impact on the global climate and the 87Sr/86Sr ratio of seawater: Earth and Planetary Science Letters, v. 188, p. 459–474.

Donnadieu, Y., Dromart, G., Goddéris, Y., Pucéat, E., Brigaud, B., Dera, G., Dumas, C., and

298 Olivier, N., 2011, A mechanism for brief glacial episodes in the Mesozoic greenhouse:
299 Paleoceanography, v. 26, p. PA3212, http://doi.wiley.com/10.1029/2010PA002100.
300 Donnadieu, Y., Goddéris, Y., Pierrehumbert, R., Dromart, G., Fluteau, F., and Jacob, R., 2006a,
301 A GEOCLIM simulation of climatic and biogeochemical consequences of Pangea breakup:
302 Geochemistry, Geophysics, Geosystems, v. 7, p. Q11019,
303 http://doi.wiley.com/10.1029/2006GC001278.
304 Donnadieu, Y., Pierrehumbert, R., Jacob, R., and Fluteau, F., 2006b, Modelling the primary
305 control of paleogeography on Cretaceous climate: Earth and Planetary Science Letters, v.
306 248, p. 426–437.
307 Dutkiewicz, A., Müller, M.D., Cannon, J., Vaughan, S., and Zahirovic, S., 2019, Sequestration
308 and subduction of deep-sea carbonate in the global ocean since the Early Cretaceous:
309 Geology, v. 47, p. 91–94, doi:10.1130/G45424.1.
310 East, M., Müller, R.D., Williams, S., Zahirovic, S., and Heine, C., 2020, Subduction history
311 reveals Cretaceous slab superflux as a possible cause for the mid-Cretaceous plume pulse
312 and superswell events: Gondwana Research, v. 79, p. 125–139,
313 doi:10.1016/j.gr.2019.09.001.
314 Engebretson, D.C., Kelley, K.P., Cashman, H.J., and Richards, M.A., 1992, 180 Million Years of
315 Subduction: GSA Today, v. 2, p. 93–100.
316 Foster, G.L., Royer, D.L., and Lunt, D.J., 2017, Future climate forcing potentially without
317 precedent in the last 420 million years: Nature Communications, v. 8, p. 14845,
318 doi:10.1038/ncomms14845.
319 Goddéris, Y., Donnadieu, Y., Le Hir, G., Lefebvre, V., and Nardin, E., 2014, The role of
320 palaeogeography in the Phanerozoic history of atmospheric CO2 and climate: Earth-Science

Reviews, v. 128, p. 122–138, doi:10.1016/j.earscirev.2013.11.004.

Gough, D.O., 1981, Solar interior structure and luminosity variations*: Solar Physics, v. 74, p. 21–34.

Gradstein, F.M., Ogg, J.G., Schmitz, M., and Ogg, G. (Eds.), 2012, The Geologic Time Scale, Volumes 1 & 2: Elsevier.

Jacob, R.L., 1997, Low frequency variability in a simulated atmosphere-ocean system: University of Wisconsin Madison, 170 p.

Kiessling, W., Flügel, E., and Golonka, J., 2000, Fluctuations in the carbonate production of Phanerozoic reefs: Geological Society Special Publication, v. 178, p. 191–215, doi:10.1144/GSL.SP.2000.178.01.13.

Kiessling, W., Flügel, E., and Golonka, J., 2003, Patterns of phanerozoic carbonate platform sedimentation: v. 36, 195–226 p., doi:10.1080/00241160310004648.

Ladant, J.-B., and Donnadieu, Y., 2016, Palaeogeographic regulation of glacial events during the Cretaceous supergreenhouse: Nature communications, v. 7, p. 12771, http://dx.doi.org/10.1038/ncomms12771.

Lanteaume, C., Fournier, F., Pellerin, M., and Borgomano, J., 2018, Testing geologic assumptions and scenarios in carbonate exploration: Insights from integrated stratigraphic, diagenetic, and seismic forward modeling: Leading Edge, v. 37, p. 672–680, doi:10.1190/tle37090672.1.

Mason, E., Edmonds, M., and Turchyn, A. V, 2017, Remobilization of crustal carbon may dominate dominate volcanic arc emissions: Science, v. 294, p. 290–294.

McKenzie, N.R., Horton, B.K., Loomis, S.E., Stockli, D.F., Planavsky, N.J., and Lee, C.-T.A., 2016, Continental arc volcanism as the principal driver of icehouse-greenhouse variability:

344 Science, v. 352, p. 444–447.
345 Van Der Meer, D.G., Zeebe, R.E., Van Hinsbergen, D.J.J., Sluijs, A., Spakman, W., and Torsvik,
346 T.H., 2014, Plate tectonic controls on atmospheric CO2 levels since the Triassic:
347 Proceedings of the National Academy of Sciences of the United States of America, v. 111,
348 p. 4380–4385, doi:10.1073/pnas.1315657111.
349 Müller, R.D., Sdrolias, M., Gaina, C., Steinberger, B., and Heine, C., 2008, Long-term sea-level
350 fluctuations driven by ocean basin dynamics: Science, v. 319, p. 1357–1362,
351 http://www.sciencemag.org/cgi/doi/10.1126/science.1151540.
352 Pall, J., Zahirovic, S., Doss, S., Hassan, R., Matthews, K.J., Cannon, J., Gurnis, M., Moresi, L.,
353 Lenardic, A., and Dietmar Müller, R., 2018, The influence of carbonate platform
354 interactions with subduction zone volcanism on palaeo-atmospheric CO2 since the
355 Devonian: Climate of the Past, v. 14, p. 857–870, doi:10.5194/cp-14-857-2018.
356 Paris, G., Donnadieu, Y., Beaumont, V., Fluteau, F., and Goddéris, Y., 2016, Geochemical
357 consequences of intense pulse-like degassing during the onset of the Central Atlantic
358 Magmatic Province: Palaeogeography, palaeoclimatology, palaeoecology, v. 441, p. 74–82,
359 http://dx.doi.org/10.1016/j.palaeo.2015.04.011.
360 Schlager, W., 2010, Ordered hierarchy versus scale invariance in sequence stratigraphy:
361 International Journal of Earth Sciences, v. 99, p. 139–151, doi:10.1007/s00531-009-0491-8.
362 Schlager, W., 1981, The paradox of drowned reefs and carbonate platforms: Geological Society
363 of America Bulletin, v. 92, p. 197–211.
364 Scotese, C.R., 2016, PALEOMAP PaleoAtlas for GPlates and the PaleoData Plotter Program
365 (PALEOMAP Project, 2016):, https://www.earthbyte.org/paleomap-paleoatlas-for-gplates/.
366 Scotese, C.R., and Wright, N., 2018, PALEOMAP Paleodigital Elevation Models (PaleoDEMS)

for the Phanerozoic (PALEOMAP Project, 2018):, https://www.earthbyte.org/paleodem-resource- scotese-and-wright-2018/.

Skelton, P.W., 2003, The operation of the major geological carbon sinks, *in* Skelton, P.W., Spicer, R.A., Kelley, S.P., and Gilmour, I. eds., The Cretaceous World, Cambridge University Press, p. 259–266.

Skelton, P.W., and Gili, E., 2011, Rudists and carbonate platforms in the Aptian: a case study on biotic interactions with ocean chemistry and climate: Sedimentology, v. 59, p. 81–117, http://doi.wiley.com/10.1111/j.1365-3091.2011.01292.x.

Strasser, A., and Samankassou, E., 2003, Carbonate sedimentation rates today and in the past: Holocene of Florida Bay, Bahamas, and Bermuda vs. Upper Jurassic and lower cretaceous of the Jura mountains (Switzerland and France): Geologia Croatica, v. 56, p. 1–18, doi:10.4154/GC.2003.01.

Veizer, J. et al., 1999, 87Sr/86 Sr, δ13 C and δ18 O evolution of Phanerozoic seawater: Chemical Geology, v. 161, p. 59–88, doi:10.1016/S0009-2541(99)00081-9.

Whitten, E.H.T., 1976, Cretaceous phases of rapid sediment accumulation, continental shelf, eastern USA: Geology, v. 4, p. 237–240, doi:10.1130/0091-7613(1976)4<237:CPORSA>2.0.CO;2.

FIGURE CAPTIONS

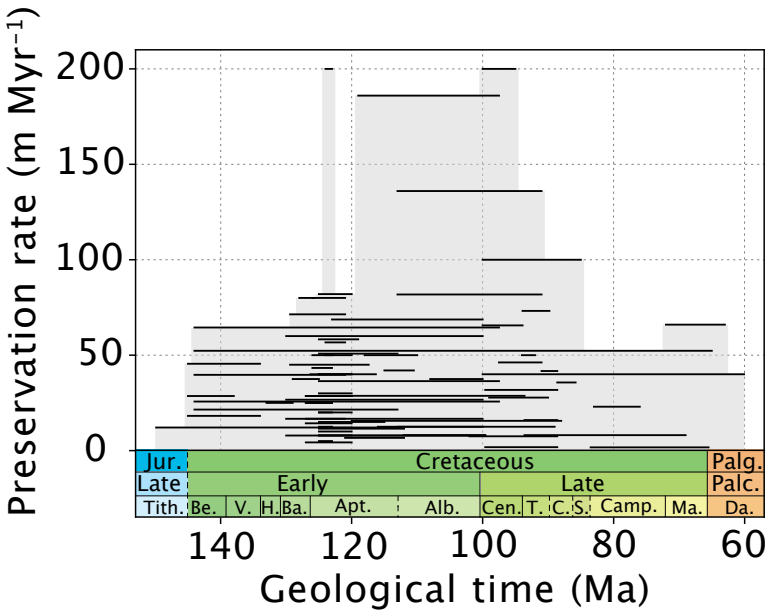

386

387 Figure 1. Compilation of Cretaceous neritic carbonate preservation rates. The light grey
388 envelope represents the maximum accumulation rates, which are likely to best represent neritic
389 carbonate production in ancient times (see Methods). Stratigraphic boundaries after Gradstein et
390 al. (2012).

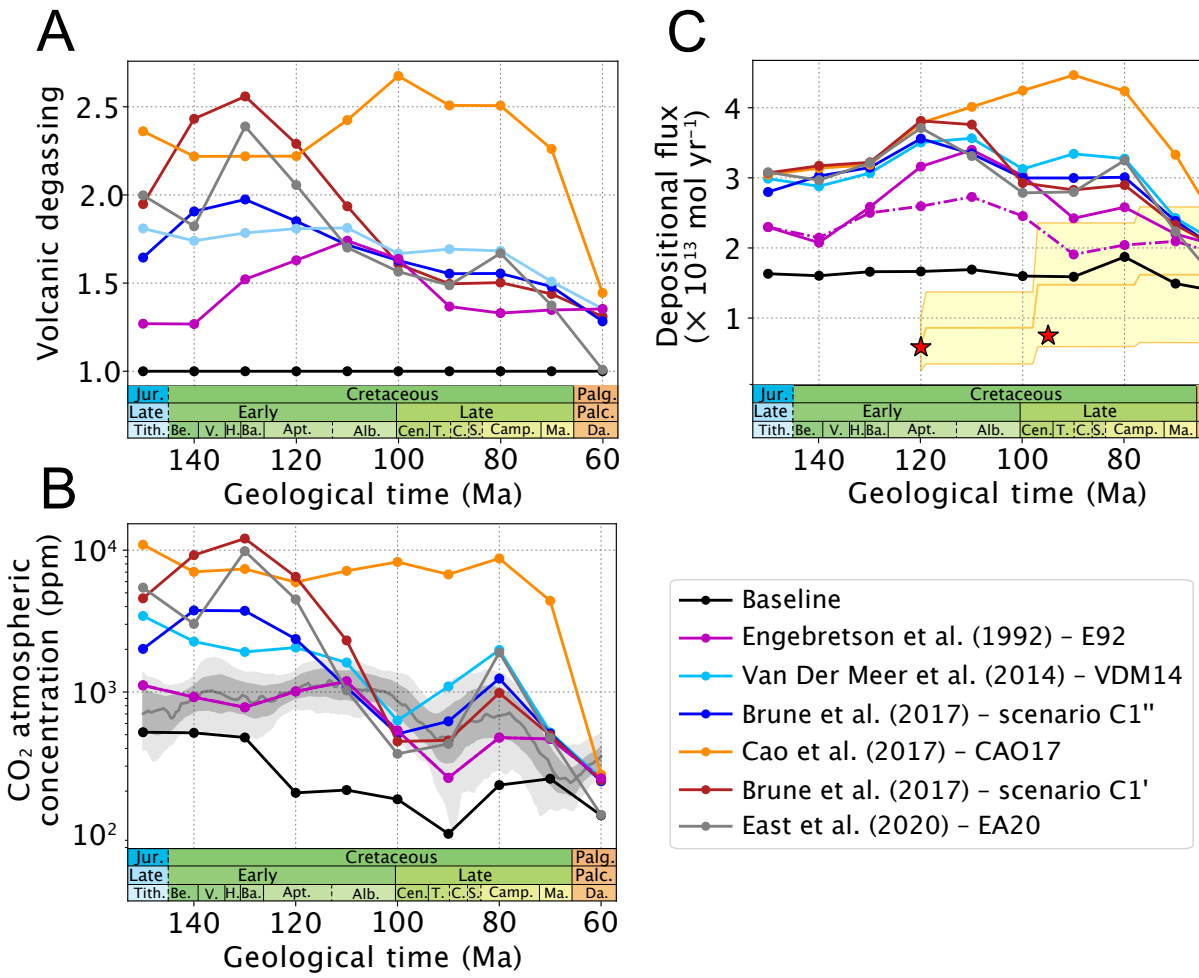

Figure 2. Model results. (A) Volcanic degassing scenarios used in the GEOCLIM model (ratio to present-day value), (B) predicted atmospheric CO_2 concentration and (C) predicted neritic carbonate total depositional flux. Black line represents the baseline runs with volcanic degassing set to the present-day level. Solid color lines represent volcanic degassing scenarios. For scenario E92, the simulation represented with the dashed line is identical to the one represented with the solid line except that it uses a constant area of the shallow-marine environments available to neritic carbonate deposition during the Cretaceous. In panel B, background grey shading represents the proxy-based pCO_2 reconstruction of Foster et al. (2017) with LOESS fit, 68 % and 95 % confidence intervals. In panel C, yellow shading and red stars

401 respectively represent the platform carbonate accumulation fluxes estimated by Dutkiewicz et al.
402 (2019) and Skelton (2003) (see main text).
403
404

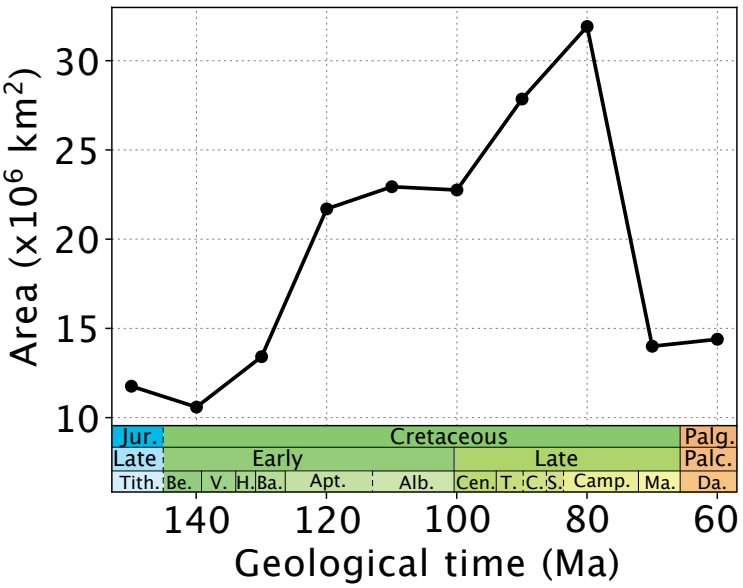

405
406 Figure 3. Area of the shallow-marine environments available to neritic carbonate
407 deposition, derived from the paleogeographical reconstructions (see the Data Repository).
408
409 [1]GSA Data Repository item 201Xxxx, [Supplementary information, geological database,
410 experimental setup and climate model runs (Sections DR1–DR2, Figures DR1–DR2, and Tables
411 DR1–DR2)], is available online at www.geosociety.org/pubs/ft20XX.htm, or on request from
412 editing@geosociety.org.